Available online at www.sciencedirect.com

ScienceDirect

Procedia Structural Integrity 18 (2019) 849–857

Structural Integrity Procedia

www.elsevier.com/locate/procedia

25th International Conference on Fracture and Structural Integrity

A study of wear and rolling contact fatigue on a wheel steel in alternated dry-wet contact aided by innovative measurement systems

Ileana Bodini[a], Angelo Mazzù[a]*, Candida Petrogalli[a], Matteo Lancini[a], Takanori Kato[b], Taizo Makino[b]

[a]*University of Brescia, Department of Mechanical and Industrial Engineering, via Branze 38, Brescia 25123, Italy*
[b]*Steel Research Laboratories, Nippon Steel Corporation, 1-8 Fuso-cho, Amagasaki, Japan*

Abstract

Wear and rolling contact fatigue are competing phenomena in railway wheels, as wear tends to shorten or remove surface cracks nucleated by ratcheting. The presence of water at the contact interface can enhance crack propagation leading to fatigue failure. This topic was studied taking advantage of innovative measurement systems developed for assessing the damage in bi-disc rolling contact tests, including a vision system for the acquisition and elaboration of surface images and a machine-learning technique for vibration measurement and analysis. Tests of different total duration with alternated dry and wet contact phases were carried out. The analysis of the collected measurements allowed identifying when crack propagation begins to prevail on wear: this occurred well earlier than the visible emergence of fatigue damage. If short dry and wet contact sessions are alternated, the onset of fluid driven crack propagation is delayed, because initially the dry sessions are not long enough to allow surface cracks to form by ratcheting, and in the subsequent wet session ratcheting is suspended due to low friction. If the alternated dry-wet contact sessions are longer, the onset of fluid driven crack propagation is accelerated, as in the dry sessions ratcheting proceeds more forming longer surface cracks, which are able to propagate in the subsequent wet phase.

Peer-review under responsibility of the Gruppo Italiano Frattura (IGF) ExCo.

Keywords: Wheel steel; Dry-wet contact; Ratcheting; Crack propagation; Vision systems; Vibration analysis.

* Corresponding author. Tel.: +39-030-3715525; fax: +39-030-3702448.
E-mail address: angelo.mazzu@unibs.it

2452-3216
Peer-review under responsibility of the Gruppo Italiano Frattura (IGF) ExCo.
10.1016/j.prostr.2019.08.235

1. Introduction

Wear and Rolling Contact Fatigue (RCF) are competing phenomena in train wheels, as shown, for instance, by Mazzù et al. (2015) an Mazzù et al. (2019). Wear is a gradual removal of material from the wheel tread and is mainly influenced by contact pressure, sliding, friction and possible presence of third bodies at the contact interface. Although wear is always present, it becomes severe in the case of high sliding and high friction, as is the case of a wheel traveling in curve in dry contact. In these cases, due to the high frictional forces, wear is usually accompanied by intense unidirectional plastic flow (ratcheting), which severely strains the steel below the contact surface leading to the formation of inclined surface cracks. RCF, in railway wheels, is usually intended as a severe damage developing through cracks that nucleate at the contact surface, propagate for some extension below the tread and finally re-emerge causing the detachment of material portions that can be also large. This phenomenon is enhanced by the presence of fluids, such as rain, grease or other, which are entrapped inside the cracks and are pressurized when the contact load closes the crack mouth and compresses the crack region, as shown by Makino et al. (2012). Crack propagation can occur only if surface crack are long enough to allow the Stress Intensity Factor (SIF) exceeding the material propagation threshold; wear, by removing material from the surface, reduces the length of the surface cracks as well, this way contrasting crack propagation.

The competition between wear and RCF has been experimentally studied by several authors. For instance, Faccoli et al. (2017) made bi-disc tests of wheel rail contact, studying the effects of fully dry contact, fully wet contact, and dry contact followed by wet contact. The last condition caused the most sudden and severe failure, because, when water was added after cycling in dry contact, the surface cracks previously generated by ratcheting rapidly propagated due to the entrapped fluid pressurization, causing severe RCF. Zhou et al. (2014) studied the interaction between wear and RCF in rails, both by field measurements and laboratory analyses, finding that under certain conditions the rails can be designed such to optimize the wear-RCF interaction and reduce damage. Ramalho et al. (2013) studied the effect of the contact conditions on friction and wear of rail and wheel steels in dry condition, by means of two-disc rolling-sliding tests. Seo et al. (2018) studied the effect of water and friction modifiers on wear and RCF of rails, finding again that both water and friction modifiers enhance fatigue crack growth by the fluid pressurization mechanism. In all of these works the wet and dry conditions were studied separately or subsequently.

The aim of this paper, instead, is to study the wear-RCF competition under alternate dry and wet contact, in order to understand what happens in the train wheels when they are subjected to the normal alternation of weather conditions. The study was carried out on a wheel steel by means of bi-disc tests of rolling and sliding contact in alternated wet and dry condition. In order to have information about the damage evolution during the test, advanced monitoring techniques, based on vision and vibration analysis, were used. The vision system was developed by Bodini et al. (2018), who proposed synthetic indexes, obtained by the analysis of images taken from the contact surface, to quantitatively evaluate the surface degradation. The vibration analysis was introduced by Lancini et al. (2015) as a monitoring system for bi-disc tests, and it was proven to be well correlated with the damage evolution, as shown by Mazzù et al. (2015) who compared this system with other measurement techniques. In this paper, a further advancement is represented by the application of machine learning techniques to vibration analysis.

2. Materials and methods

The tests were carried out by means of the bi-disc testing machine shown in Fig. 1, whose detailed description is provided by Bodini et al. (2018). It is a bi-disc machine where the specimens are fixed to independent shafts. One of them can be displaced orthogonally to the shaft axis by a hydraulic cylinder, which applies the imposed contact load as well. The rolling speed of each shaft is measured by encoders, whereas a load cell located at the piston head measures the contact load between specimens. Two piezo-accelerometers are mounted on the specimen supports: one on the fixed shaft in vertical direction and the other one on the mobile shaft in horizontal direction, both normal to the rotation axis. The used transducers are Wilcoxon 736 IEPE accelerometers, with nominal sensitivity 0.98 V/(m/s^2), full scale 5 m/s^2, linear bandwidth within the range 5-20k Hz. A Steiger-Mohilo 0225DF torque sensor is mounted at the mobile shaft, with maximum nominal torque 2000 N m and accuracy class 0.2.

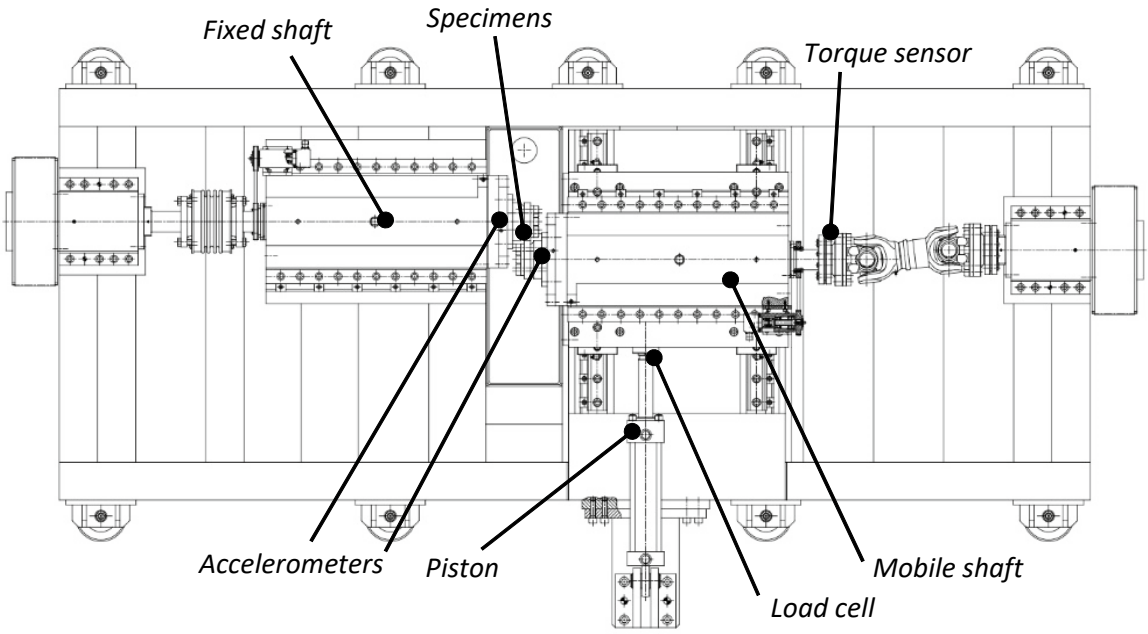

Fig. 1. Schematic of the bi-disc test bench.

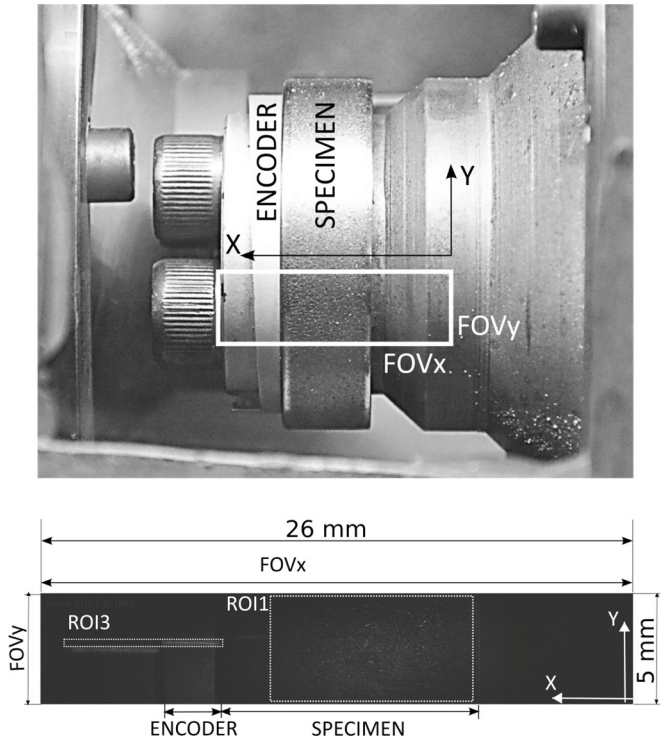

Fig. 2. Analogic, linear encoder fixed on a disk coaxially screwed on the specimen. Definition of the X and Y directions

The vision system, mounted on the test bench, includes a high-speed camera (PROMON 501; AOS Technologies AG) with a f/50 mm lens, two laser pointers suitably defocused to illuminate the specimen surface, and a laser blade illuminating an encoder purposely designed. This component is an axial cam, with external diameter of 50 mm and internal diameter of 44 mm (see Fig. 2); the height of the region with the maximum diameter varies linearly along the circumference from 3 mm to 8 mm. The camera acquires images with dimensions (1280 px × 240 px), with a bit depth of 8 bit, and the resulting field of view (FOV) is (26 mm × 6.5 mm) with spatial resolution equal to 0.021 mm/px, in both X and Y directions. During the dry tests, images of the surface of the wheel specimens were continuously acquired at a frequency of 377 fps. They were acquired with a gain of 24 and an exposure time of 40 μs. In the performed tests, surface images of rolling wheel specimens are acquired every 10 seconds, each acquisition having a duration of 2 seconds. Acquisitions are also performed at the beginning and at the end of each step, with the mandrel rotating at the reduced speed of 5 rpm. In these cases, the acquisition frequency of the vision-based measurement system is 100 fps and the duration of the acquisition is 1 min, as specified in Bodini et al. (2016).

Six rolling-sliding tests in dry and wet contact were carried out on specimens in 0.7%C steel with fine pearlite structure, with hardness HV330. All of the tests were conducted with the same maximum contact pressure (0.9 GPa), rolling speed (500 rpm) and sliding/rolling ratio (0.5%). Wet contact was realized by means of a jet of water with the addition of 10% glycol. A summary of the applied test conditions in terms of sequence of dry and wet sessions is shown in

Table 1. The tests were stopped when severe damage occurred on the surface: this condition was identified by a severe increment of the vibrations of the mobile mandrel, as detailed below in the results section.

Table 1: Summary of the applied test conditions.

Test ID	Dry-wet sequence
K2	50.000 dry + 50.000 wet + 50.000 dry + 50.000 wet + … up to failure
K4	50.000 dry + 50.000 wet + 50.000 dry + 50.000 wet + … up to failure
K6	600.000 dry + n wet up to failure
K8	1.000.000 dry + n wet up to failure
K13	100.000 dry + 100.000 wet + 100.000 dry + 100.000 wet + … up to failure
K14	200.000 dry + 200.000 wet + 200.000 dry + 200.000 wet + … up to failure

Images of the surface of the specimen undergo simple and fast image processing to quantify surface damage, allowing the definition and assessment of synthetic indexes. Two regions of interest (ROI) were defined, shown in Fig. 2: ROI1 includes the surface of the specimen illuminated by the defocused lasers; ROI3 includes the encoder surface illuminated by the laser blade, from which the angular position is obtained after determining the laser blade length according to the procedure detailed by Bodini et al. (2018). ROI1 is illuminated by a diffused light, which results in a scattered light pattern on the specimen surface, whose images exhibit bright areas having number, dimension, position, shape and orientation that can be correlated to the formation of small dips and crests during wear and RCF processes. To analyze such non-texturized discrete defects, blob analysis is used. A blob is each pixel group within a closed line: in the presented work, blobs correspond to bright areas and, to highlight them, each image underwent firstly a thresholding process detailed by Bodini et al. (2018). Blob analysis allows the parameter *RB*, defined as follows:

$$R_B = \frac{A_B}{A_{ROI1}} \tag{1}$$

where A_B is the sum of the areas of the blobs found in the region ROI1, averaged over the whole specimen surface, and A_{ROI1} is the total area of ROI1.

Vibrations and torque measurement are post-processed as deeply explained by Bini Chiesa et al. (2018). Measurements acquired from the accelerometers mounted on the specimens' supports and from the torque sensor are processed in data packets of 0.2 s each. From each packet, made up by 1000 samples per channel, a set of synthetic features are extracted. The features extracted from each channel are: mean, standard deviation, variance, RMS,

percentiles, centroid of the Power Spectrum Density. Taking into account every combination of channel pair, then, the maximum value of the cross-correlation and its time delay, the centroid of the Frequency Response Function and frequency quartiles are computed. All the features have been normalized with the Z-Score method: by subtracting the average of its values and dividing by the standard deviation. Then the number of features has been reduced through a Principal Component Analysis (PCA), setting a threshold for selection equal to 90% of the variance.

Then a K-means algorithm is applied to the selected features, setting K between 2 and 4. The algorithm is unsupervised, so it requires no reference state or condition and simply classifies the current state of the specimen (given by the combination of vibrations and torque information) by computing the probability of belonging to a set of clusters iteratively defined by the process itself. This "membership probability" is obtained by normalizing the square distance between the current state and the clusters centres in the feature space. While not directly associated with a physical condition, monitoring this probability in time during the tests can identify when the phenomena involved in RCF tests change their behaviour.

3. Experimental results

3.1. Image analysis

Each test was stopped when the surface was severely damaged; this condition was identified by a significant increment of the vibrations of the mobile mandrel, exceeding 2 m/s^2.

Fig. 3 shows the R_B parameter for all of the tests. Filled triangles refer to the measurements after the dry phase, empty dots after the wet one. In the test K2, initially R_B is generally higher after the dry sessions than after the wet ones (with some exceptions), meaning that the vision system recognizes a more perturbed surface appearance after the formers. This tendency is inverted after 700000 cycles: indeed, in the final part of the test R_B is higher after the wet session than after the dry one. A similar behavior can be observed in the test K4 after about 900000 cycle, although the overall values of R_B are lower than in the previous test: this is due to the fact that R_B is averaged over the whole contact surface, whereas in this test the damage involved a part of it. In test K6, when water was added after a 600000 cycle dry session, the R_B raised suddenly. In test K8, which was characterized by a 1 million cycle long dry session, the R_B value was slightly progressing during dry session, as highlighted by the trend line; the application of water did not cause a significant variation. In test K13 the inversion of tendency became evident after 800000 cycles; in test K14 after 700000 cycles.

3.2. Vibration analysis

Vibration and torque measurements were synthesized into features, as explained in the previous chapter, and this allowed a machine-learning algorithm to classify each recorded sample into four different clusters. Fig. 4 shows the time variation of the probability associated to each sample to belong to each cluster in each test. Changes of tendency of these lines are sign of a change of state in the test, although this cannot give information about what exactly is changing. Colors and legend are not coherent between the various diagrams, since the cluster number is automatically assigned by the classification algorithm, without a reference indication to be used as label. The general information provided by these diagrams is, however, already clear, in particular if we consider that the cluster present at the beginning of the test is more likely to be related to a pristine condition of the specimen, while the cluster detected at the end of the test could be associated with a damaged state. In test K2, the cluster 1 seems to be associated to the final failure, as it suddenly rises at the end of the test. Considering the other clusters, instead, we can notice an inversion of tendency at about 700000 cycles, when the cluster 3 becomes dominant with respect to cluster 2 and cluster 4. This number of cycles is approximately the same as that corresponding to the inversion of tendency of the R_B parameter. In test K4 the same tendency can be observed for cluster 1, which rapidly rises at the end of the test. For the other clusters, again a change of state seems to appear at 900000 cycles, although it is less clear than in the previous test. The number of cycles associated with this change of state, again, is coherent with the R_B diagram. In test K6, again the green and yellow lines show an inversion of tendency corresponding to the beginning of the wet session, consistently with the R_B diagram. In test K8, two state changes appear: one after 450000 cycles (inversion of green and yellow lines) and another one after 1000000 cycles (raise of the red line). The second change can be associated to

the application of water; the first one is more gradual than in other tests, in agreement with the R_B parameter behavior. In tests K13 the inversion of tendency is after about 450000 cycles, in test K14 it is clearly evident after about 420000 cycles. In these last two test the inversion of tendency revealed by the vibration analysis is anticipated with respect to the image analysis, but this is compatible with the fact that the former is continuously acquired, the latter after long intervals.

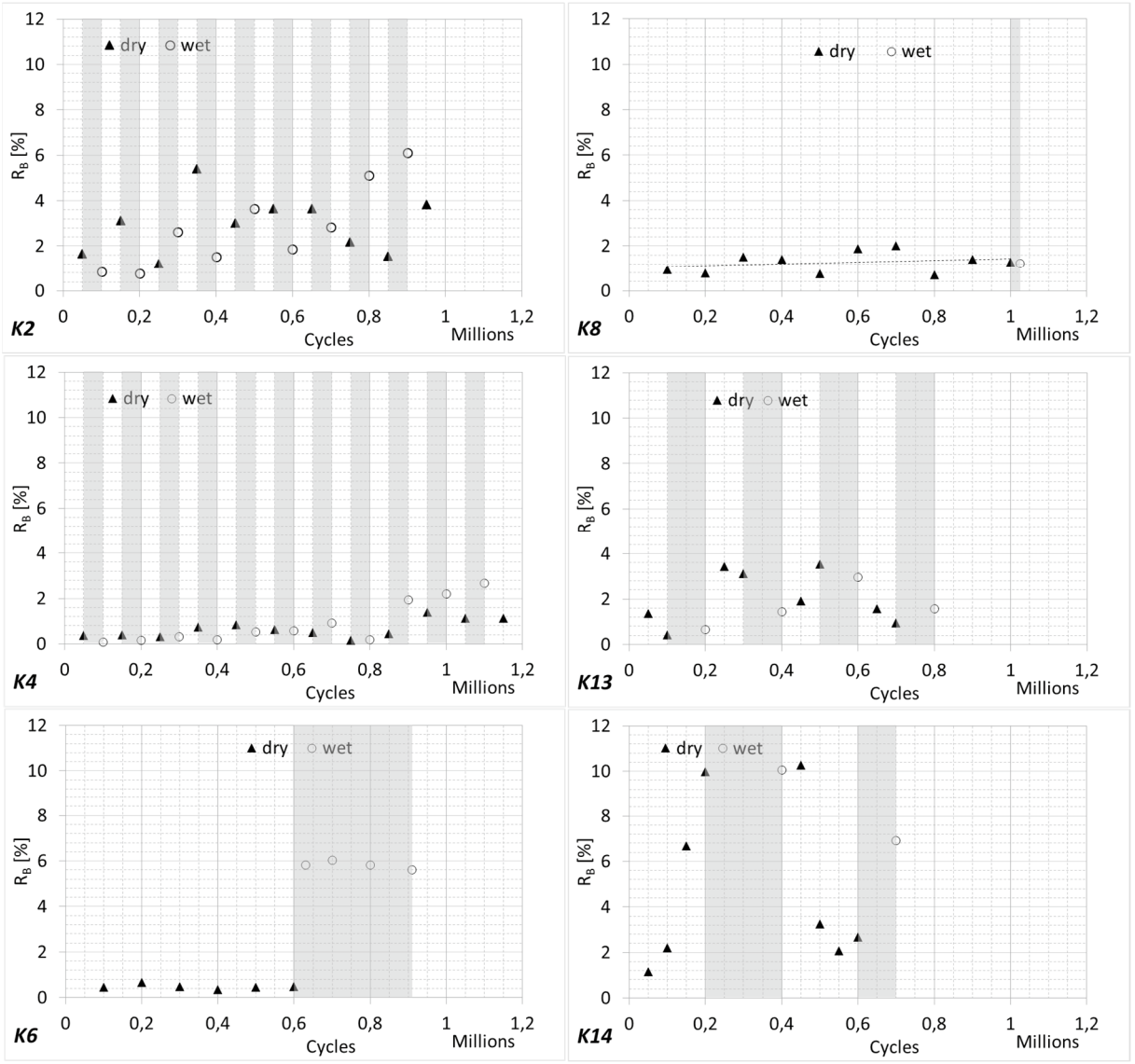

Fig. 3. : R_B parameter during the tests. Grey bands correspond to wet contact sessions.

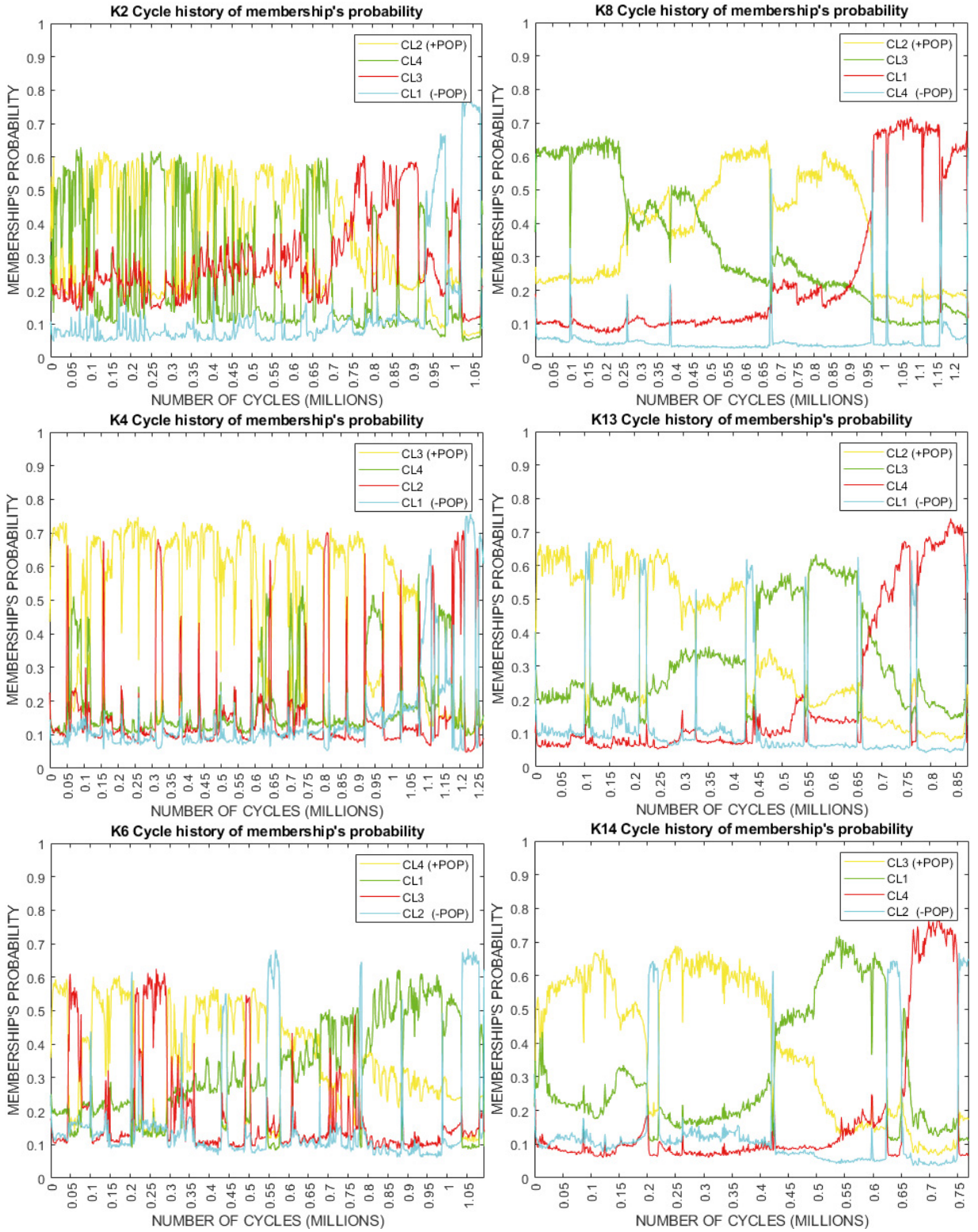

Fig. 4: Membership probability during the tests. Cluster numbering depends on each test.

4. Discussion

The results of the image analysis can be put in relationship with the damage phenomena occurring at the contact surface, studied in several previous works. As introduced above, in sliding dry contact ratcheting and wear are the prevailing damage mechanisms, which initially cause plastic flow, corrugations and small surface cracks with a low inclination with respect to the contact surface: this explains the increment of R_B after the dry sessions. When water is added, the coefficient of friction lowers and ratcheting probably arrests or slows down; on the contrary, it is probable that local contact between asperities tends to smooth the contact surface, thus explaining the lowering of R_B. However, ratcheting restarts at each dry session, increasing the depth and the slope of the surface cracks; when they are long enough, in the wet sessions the mechanism of crack propagation due the entrapped fluid pressurization can be activated. When this happens, the effect of the wet and dry sessions on the surface degradation is inverted: wet sessions increase the damage due to crack propagation, whereas dry sessions mitigate this effect by means of wear that, by removing material layers from the surface, reduces the length of the cracks previously propagated. This explains why, after a certain number of cycles, there is an inversion of the tendency of R_B, which is confirmed by the tendency revealed by the vibration analysis.

In test K2 the inversion occurs after 700000 cycles, e.g. 350000 total dry cycles and 350000 total wet cycles. In test K4 the inversion occurs after about 900000 cycles, e.g. 450000 total dry cycles and 450000 total wet cycles. In test K6 the inversion occurs as soon as the water is added, e.g. after 600000 dry cycles. In test K8 the first inversion is revealed only by the vibration analysis, and occurs after about 450000 dry cycles, but in this case this datum cannot be related to wet-dry contact alternation. In tests K13 and K14 the inversion occurs after 450000 and 400000 cycles respectively, e.g. 250000-200000 total dry cycles and 200000 total wet cycles. Overall, these results suggest that the alternation of brief phases of wet and dry contact mitigates fatigue. In fact, in tests with initial long dry sessions (K6 and K8) fluid driven crack propagation started as soon as water was added, leading rapidly to failure; on the contrary, in tests K2 and K4, characterized by alternated short wet-dry contact session, the onset of crack propagation was delayed. This can be explained with the fact that the fluid mitigates ratcheting in the wet session and wear slightly mitigates the surface corrugation in the wet sessions. However, if the alternated contact sessions are longer, as in tests K13 and K14, the onset of fatigue is anticipated. This can be related to the fact that in dry sessions the ratcheting advances more, increasing the probability of forming surface cracks long enough to start propagation in the subsequent wet phase; on the other hand, as even the wet sessions are longer, cracks can propagate more by the entrapped fluid pressurization before being shortened by wear in dry contact.

5. Conclusions

Rolling contact tests in alternated dry-wet contact were carried out by means of a bi-disc test bench, under the same contact pressure and sliding speed, with varying duration of the alternated dry and wet phases. The tests were monitored by means of image and vibration analyses, which were able to reveal state changes in the specimens before the damage became severe enough to be detectable with traditional measuring systems.

The analyses suggested that if short dry and wet contact sessions are alternated, the onset of fluid driven crack propagation is delayed, because initially the dry sessions are not long enough to allow surface cracks to form by ratcheting, and in the subsequent wet session ratcheting is suspended due to low friction. However, if the alternated dry-wet contact sessions are longer, the onset of fluid driven crack propagation is accelerated: in fact, in the dry sessions ratcheting proceeds more forming longer surface cracks, which in the subsequent wet phase have more cycles to propagate due to the entrapped fluid pressurization. In other words, if the alternated contact sessions are short, the damage mitigation effect of wear in dry sessions and of low friction in wet sessions is maximized; if the alternated contact sessions are long, the damage enhancing effect of ratcheting in dry sessions and of entrapped fluid pressurization in wet sessions is maximized.

Acknowledgements

We are grateful to Silvio Bonometti and Gabriele Coffetti for their technical support.

References

Bini Chiesa, M., Bodini, I., Petrogalli, C., Provezza, L., Faccoli, M., Mazzu, A., Solazzi, L., Sansoni, G., Lancini, M., K-means clustering approach for damage evolution monitoring in RCF test, Journal of Physics Conferences Series, 1065(10); 102018

Bodini, I., Petrogalli, C., Faccoli, M., Lancini, M., Pasinetti, S., Sansoni, G., Docchio, F., Mazzù, A., 2018. Evaluation of Wear in Rolling Contact Tests by Means of 2D Image Analysis. Wear 400-401, 156-168.

Bodini I., Sansoni G., Lancini M., Pasinetti S., Docchio F., 2016, A novel optical apparatus for the study of rolling contact wear/fatigue based on a high-speed camera and multiple-source laser illumination, Review of Scintific Instruments, 87(8), 083701

Faccoli, M., Petrogalli, C., Lancini, M., Ghidini, A., Mazzù, A., 2017. Rolling Contact Fatigue and Wear Behavior of High-Peformance Railway Wheel Steels under Various Rolling-Sliding Contact Conditions. Journal of Material Engineering and Performance 26(7), 3271–3284.

Lancini, M., Bodini, I., Vetturi, D., Pasinetti, S., Mazzù, A., Solazzi, L., Petrogalli, C., Faccoli, M., 2015. Using Vibration Measurements to Detect High Wear Rates in Rolling ContactFatigue Tests. Acta IMEKO 4(4), 66-74.

Makino, T., Kato, T., Hirakawa, K., 2012. The Effect of Slip Ratio on the Rolling Contact Fatigue Property of Railway Wheel Steel. International Journal of Fatigue 36(1), 68-79.

Mazzù, A., Petrogalli, C., Faccoli, M., 2015. An Integrated Model for Competitive Damage Mechanisms Assessment in Railway Wheel Steels. Wear 322-323, 181–191.

Mazzù, A., Solazzi, L., Lancini, M., Petrogalli, C., Ghidini, A., Faccoli, M., 2015. An Experimental Procedure for Surface Damage Assessment in Railway Wheel and Rail Steels. Wear 342-343, 22-33.

Mazzù, A., Petrogalli, C., Lancini, M., Ghidini, A., Faccoli, M., 2018. Effect of Wear on Surface Crack Propagation in Rail-Wheel Wet Contact. Journal of Material Engineering and Performance 27(2), 630–639.

Ramalho, A., Esteves, M., Marta, P., 2013. Friction and Wear Behaviour of Rolling–Sliding Steel Contacts. Wear 302 (2013), 1468-1480.

Seo, J. W., Jun, H. K., Kwon, S. J., Lee, D. H., 2018. Effect of Friction Modifier on Rolling Contact Fatigue and Wear of Wheel and Rail Materials. Tribology Transactions 61(1), 19-30.

Zhou, Y., Wang, S., Wang, T., Xu, Y., Li, Z., 2014. Field and Laboratory Investigation of the Relationship Between Rail Headcheck and Wear in a Heavy-Haul Railway. Wear 315, 68-77.